

## Near Infrared Plasmonic Enhanced Solar Energy Harvest for Highly Efficient Photocatalytic Reactions

Jiabin Cui, Yongjia Li, Lei Liu, Lin Chen, Jun Xu, Jingwen Ma, Gang Fang, Enbo Zhu, Hao Wu, Lixia Zhao, Leyu Wang, and Yu Huang

*Nano Lett.*, **Just Accepted Manuscript** • DOI: 10.1021/acs.nanolett.5b00950 • Publication Date (Web): 07 Sep 2015

Downloaded from <http://pubs.acs.org> on September 11, 2015

### Just Accepted

“Just Accepted” manuscripts have been peer-reviewed and accepted for publication. They are posted online prior to technical editing, formatting for publication and author proofing. The American Chemical Society provides “Just Accepted” as a free service to the research community to expedite the dissemination of scientific material as soon as possible after acceptance. “Just Accepted” manuscripts appear in full in PDF format accompanied by an HTML abstract. “Just Accepted” manuscripts have been fully peer reviewed, but should not be considered the official version of record. They are accessible to all readers and citable by the Digital Object Identifier (DOI®). “Just Accepted” is an optional service offered to authors. Therefore, the “Just Accepted” Web site may not include all articles that will be published in the journal. After a manuscript is technically edited and formatted, it will be removed from the “Just Accepted” Web site and published as an ASAP article. Note that technical editing may introduce minor changes to the manuscript text and/or graphics which could affect content, and all legal disclaimers and ethical guidelines that apply to the journal pertain. ACS cannot be held responsible for errors or consequences arising from the use of information contained in these “Just Accepted” manuscripts.



# Near Infrared Plasmonic Enhanced Solar Energy Harvest for Highly Efficient Photocatalytic Reactions

Jiabin Cui,<sup>1†</sup> Yongjia Li,<sup>2†</sup> Lei Liu,<sup>3</sup> Lin Chen,<sup>1</sup> Jun Xu,<sup>1</sup> Jingwen Ma,<sup>1</sup> Gang Fang,<sup>1</sup> Enbo Zhu,<sup>2</sup> Hao Wu,<sup>2</sup> Lixia Zhao,<sup>3</sup> Leyu Wang,<sup>1\*</sup> and Yu Huang<sup>2\*</sup>

<sup>1</sup>State Key Laboratory of Chemical Resource Engineering, Beijing University of Chemical Technology, Beijing 100029, P. R. China; <sup>2</sup>Department of Materials Science & Engineering, University of California Los Angeles, CA 90095 USA; <sup>3</sup>Semiconductor Lighting Technology Research and Development Center, Institute of Semiconductors, Chinese Academy of Sciences, Beijing 100083, P.R. China.

\* E-mail: lywang@mail.buct.edu.cn (Professor Leyu Wang); yhuang@seas.ucla.edu (Professor Yu Huang).

†: These two authors contributed equally to the manuscript.

**KEYWORDS:** Heteronanostructures; Solar photocatalysis; Localized surface plasmon resonances (LSPR); Copper sulfide

**ABSTRACT.** We report a highly efficient photocatalyst comprised of Cu<sub>7</sub>S<sub>4</sub>@Pd heteronanostructures with plasmonic absorption in the near infrared (NIR)-range. Our results indicated that the strong NIR plasmonic absorption of Cu<sub>7</sub>S<sub>4</sub>@Pd facilitated hot carrier transfer from Cu<sub>7</sub>S<sub>4</sub> to Pd, which subsequently promoted the catalytic reactions on Pd metallic surface.

1  
2  
3 We confirmed such enhancement mechanism could effectively boost the sunlight utilization in  
4 a wide range of photocatalytic reactions, including the Suzuki coupling reaction, hydrogenation  
5 of nitrobenzene, and oxidation of benzyl alcohol. Even under irradiation at 1500 nm with low  
6 power density ( $0.45 \text{ W/cm}^2$ ), these heteronanostructures demonstrated excellent catalytic  
7 activities. Under solar illumination with power density as low as  $40 \text{ mW/cm}^2$ , nearly 80-100% of  
8 conversion was achieved within 2 hours for all three types of organic reactions. Furthermore,  
9 recycling experiments showed the  $\text{Cu}_7\text{S}_4@\text{Pd}$  were stable and could retain their structures and  
10 high activity after five cycles. The reported synthetic protocol can be easily extended to other  
11  $\text{Cu}_7\text{S}_4@\text{M}$  (M=Pt, Ag, Au) catalysts, offering a new solution to design and fabricate highly  
12 effective photocatalysts with broad material choices for efficient conversion of solar energy to  
13 chemical energy in an environmentally friendly manner.  
14  
15  
16  
17  
18  
19  
20  
21  
22  
23  
24  
25  
26  
27  
28  
29  
30  
31  
32

33 The direct conversion of solar energy to chemical energy using photocatalysts has received  
34 significant attention. Up to now, semiconductor-semiconductor, semiconductor-metal and  
35 bimetal heteronanostructures have emerged as promising photocatalysts for photodegradation of  
36 organic contaminants,<sup>1-3</sup> hydrogen generation,<sup>4-8</sup> conversion of  $\text{CO}_2$ ,<sup>9</sup> and organic synthetic  
37 reactions.<sup>10-12</sup> For example, palladium-based nanostructures have been widely employed for the  
38 catalytic reaction including the hydrogenation of nitrobenzene, oxidation of benzyl alcohol and  
39 Suzuki coupling reaction due to their excellent catalytic activity.<sup>7, 10, 11, 13, 14</sup> In order to enhance  
40 the catalytic activity and reduce the dosage of noble metal, a number of synthetic strategies have  
41 been developed to fabricate nanostructures with open surface features such as desired active  
42 facets,<sup>15-17</sup> porous structures,<sup>11, 12</sup> concave surfaces,<sup>18-20</sup> and nanoframe structures with small  
43 sizes.<sup>21-23</sup> In terms of photocatalyst design, more and more research efforts have been given to  
44  
45  
46  
47  
48  
49  
50  
51  
52  
53  
54  
55  
56  
57  
58  
59  
60

1  
2  
3 improve direct utilization of sunlight in the visible region.<sup>24-26</sup> In addition, to enhance the light  
4 conversion efficiency, localized surface plasmon resonances (LSPR), arising from the collective  
5 oscillation of free carriers in the individual nanostructure stimulated by incident light, has been  
6 widely modeled and explored in noble metal nanostructures<sup>5, 27-31</sup> for plasmonic photocatalysis,<sup>10,</sup>  
7  
8  
9  
10  
11  
12  
13  
14  
15  
16  
17  
18  
19  
20  
21  
22  
23  
24  
25  
26  
27  
28  
29  
30  
31  
32  
33  
34  
35  
36  
37  
38  
39  
40  
41  
42  
43  
44  
45  
46  
47  
48  
49  
50  
51  
52  
53  
54  
55  
56  
57  
58  
59  
60

13, 25, 27, 28, 32 sensors<sup>31, 33, 34</sup> and photothermal ablation<sup>35, 36</sup> applications.

Although noble metal nanostructure can be used alone as LSPR component and catalyst,<sup>25-27</sup> the  
semiconductor-metal heteronanostructures are relatively cheap, and can offer higher light  
harvesting efficiency. To date, CeO<sub>2</sub>-Au,<sup>37</sup> Cu<sub>2</sub>O-Au,<sup>38</sup> TiO<sub>2</sub>-Au,<sup>39</sup> CeO<sub>2</sub>-Pt<sup>40</sup> and CdS-Pt<sup>41</sup>  
heteronanostructures have been developed for photocatalytic H<sub>2</sub> generation. ZnO-Au,<sup>42</sup>  
Cu<sub>2</sub>ZnSnS<sub>4</sub>-Pt<sup>6</sup> and Cu<sub>2</sub>O-Au<sup>43</sup> heteronanostructures have been utilized for photodegradation of  
organic pollutants. All of them mainly make use of the visible or ultraviolet range irradiation  
light as energy source. According to the energy distribution in the solar spectrum, around 54.3%,  
38.9% and 6.8% of sunlight at the earth's surface is located in the near-infrared (NIR, 760-3000  
nm), visible (Vis, 400-760 nm), and ultraviolet (UV, <400 nm) range, respectively.<sup>44</sup> Therefore,  
the development of semiconductor-noble metal heteronanostructures with NIR absorption, low  
cost, high stability, and outstanding catalytic performance is still critical and highly desirable for  
efficient solar photosynthesis. The copper chalcogenide nanocrystals demonstrating excellent  
tunable plasmonic absorption especially in the NIR region are promising candidates for building  
plasmon enhanced photocatalysts. Besides, their potential as organic reaction catalysts has not  
yet been fully explored.<sup>45-49</sup>

1  
2  
3  
4  
5  
6  
7  
8  
9  
10  
11  
12  
13  
14  
15  
16  
17  
18  
19  
20  
21  
22  
23  
24  
25  
26  
27  
28  
29  
30  
31  
32  
33  
34  
35  
36  
37  
38  
39  
40  
41  
42  
43  
44  
45  
46  
47  
48  
49  
50  
51  
52  
53  
54  
55  
56  
57  
58  
59  
60

Herein, for the first time, we report a facile wet-chemistry strategy to synthesize heteronanostructure photocatalyst containing both noble metal (Pd) and Cu<sub>7</sub>S<sub>4</sub> domains with intimate interfacial contact. These Cu<sub>7</sub>S<sub>4</sub>@Pd nanocrystals, by combining NIR LSPR light-harvesting property of Cu<sub>7</sub>S<sub>4</sub> with the catalytic features of Pd, are excellent catalysts for solar photocatalysis of organic synthesis reactions. The LSPR effect enhanced photocatalytic activities of the Cu<sub>7</sub>S<sub>4</sub>@Pd heteronanostructures have been confirmed by both simulation studies and experimental evaluations through a series of organic reactions including Suzuki coupling reaction, selective oxidation of benzyl alcohol and hydrogenation of nitrobenzene.

In a typical synthesis, Cu<sub>7</sub>S<sub>4</sub> nanocrystals were prepared by solvothermal decomposition of the single precursor Cu(S<sub>2</sub>CNBut<sub>2</sub>)<sub>2</sub> containing both copper and sulfur dissolved in oleylamine.<sup>50</sup> The synthesis of Cu<sub>7</sub>S<sub>4</sub>@Pd was accomplished following a typical hot-injection method by introducing noble metal precursor Pd(S<sub>2</sub>CNBut<sub>2</sub>)<sub>2</sub> into the as-prepared Cu<sub>7</sub>S<sub>4</sub> colloids. All synthetic steps were carried out under air-free conditions (see Supporting Information for details). Figure 1 shows the transmission electron microscopy (TEM) image and high resolution transmission electron microscopy (HRTEM) image of Cu<sub>7</sub>S<sub>4</sub>@Pd. The average size of Cu<sub>7</sub>S<sub>4</sub> is 14 nm and the size of Pd particles grown inside is 4.3 nm. For each Cu<sub>7</sub>S<sub>4</sub> nanoparticle, more than one Pd particle can be found attached to the surface. The HRTEM image (Figure 1b) demonstrates an interplanar distance of 0.193 nm in semiconductor domain, consistent with the (0 16 0) lattice spacing of anilite Cu<sub>7</sub>S<sub>4</sub>. In the noble metal domains, an interplanar distance of 0.224 nm indicates the face-centered cubic (fcc) Pd (111) planes. HRTEM results also reveal the intimate metal-semiconductor interface in the heteronanostructure, which is highly favorable for charge transfer in between.<sup>51</sup> In comparison, TEM images of Cu<sub>7</sub>S<sub>4</sub> nanoparticles and Pd

1  
2  
3 nanoparticles are shown in Figure S1. The crystallinity of the semiconductor domains and noble  
4 metal domains was further examined through powder X-ray diffraction (XRD) patterns (Figure  
5 1c). The two distinct sets of diffraction peaks can be assigned to the anilite  $\text{Cu}_7\text{S}_4$  (JCPDS card  
6 23-0958, Table S1) and Pd (JCPDS card 46-1043), respectively. Therefore, both TEM images  
7 and XRD patterns confirm the successful synthesis of the desired heteronanostructures.  
8 Furthermore, other heteronanostructures including  $\text{Cu}_7\text{S}_4@Au$ ,  $\text{Cu}_7\text{S}_4@Pt$ , and  $\text{Cu}_7\text{S}_4@Ag$  can  
9 be prepared following similar procedures (see Supporting Information for details). By analyzing  
10 XRD patterns and HRTEM images, we also verified those heteronanostructures are composed of  
11 anilite  $\text{Cu}_7\text{S}_4$  and noble metal components, with good crystallinity and tight interfacial  
12 connection (Figure S2-S3).  
13  
14  
15  
16  
17  
18  
19  
20  
21  
22  
23  
24  
25  
26  
27  
28  
29  
30  
31  
32  
33  
34  
35  
36  
37  
38  
39  
40  
41  
42  
43  
44  
45  
46  
47  
48  
49  
50  
51  
52  
53  
54  
55  
56  
57  
58  
59  
60

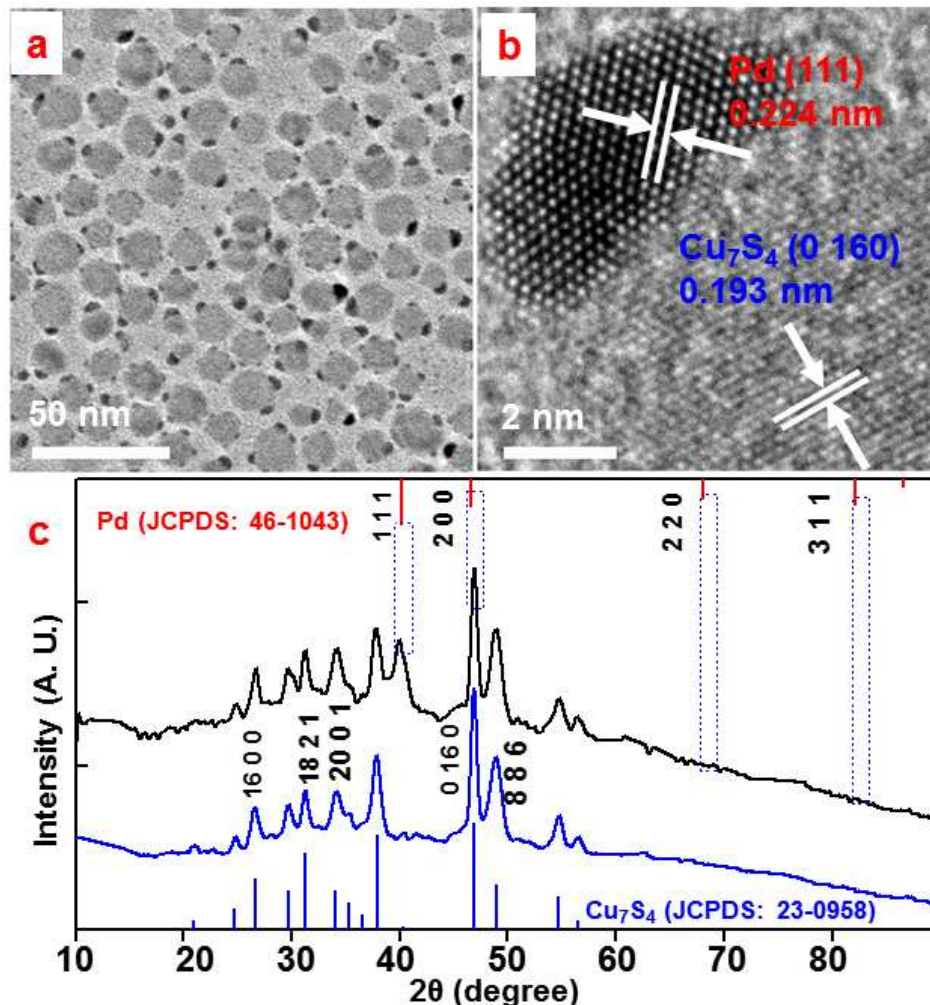


**Figure 1.** (a) TEM and (b) HRTEM images of Cu<sub>7</sub>S<sub>4</sub>@Pd. (c) XRD patterns of Cu<sub>7</sub>S<sub>4</sub>@Pd (black curve) and Cu<sub>7</sub>S<sub>4</sub> (blue curve).

The LSPR absorption spectra of Cu<sub>7</sub>S<sub>4</sub>@Pd, Cu<sub>7</sub>S<sub>4</sub> and Pd were measured experimentally (Figure 2a), and simulated by Finite Difference Time Domain (FDTD) method (Figure 2b). Pd demonstrates no LSPR peak above 1000 nm, while pure Cu<sub>7</sub>S<sub>4</sub> or physical mixture of Cu<sub>7</sub>S<sub>4</sub> and Pd gives clear absorption peak around 1500 nm, which can be observed from simulation as well. Moreover, the Cu<sub>7</sub>S<sub>4</sub>@Pd heteronanostructure demonstrates a red shift (~500 nm from

1  
2  
3 experimental result) in LSPR peak with respect to that of  $\text{Cu}_7\text{S}_4$ . It has been reported that LSPR  
4 intensity in  $\text{Cu}_7\text{S}_4$  heavily relies on free carrier density in the form of cation deficiencies.<sup>52</sup> Pd  
5 growth on  $\text{Cu}_7\text{S}_4$  surface can possibly bond with sulfur atoms and reduce the exposure of  $\text{Cu}_7\text{S}_4$   
6 to oxygen, which might annihilates vacancies in  $\text{Cu}_7\text{S}_4$ , resulting in LSPR peak red-shift.<sup>52</sup> We  
7 may also relate the red-shift to the refractive index change originated from the incorporation of  
8 Pd to LSPR surface, as observed by other groups.<sup>53,54</sup> Additionally, peak broadening effect of  
9 heteronanostructures were observed in both experimental and simulation results with reference to  
10 pure  $\text{Cu}_7\text{S}_4$  and the mixture of  $\text{Cu}_7\text{S}_4$  and Pd. Again it can be attributed to the larger dielectric  
11 constant of Pd compared to that of the solvent.<sup>52-55</sup> We also note the experimental spectrum of  
12 the  $\text{Cu}_7\text{S}_4@\text{Pd}$  heteronanostructures differs from the FDTD simulation spectrum in terms of peak  
13 position and peak width. We postulate this difference as a result of the inhomogeneous structure  
14 and size distribution of the real heteronanostructure sample, similar to previously reported  
15 phenomena.<sup>56-61</sup>

16  
17  
18  
19  
20  
21  
22  
23  
24  
25  
26  
27  
28  
29  
30  
31  
32  
33  
34  
35  
36  
37  
38 LSPR effect is generally believed to be manifested in local electrical field enhancement.<sup>46</sup> To  
39 demonstrate the presence of this enhancement spatially and study its correlation with various  
40 wavelengths, the two-dimensional (2D) contour of the electron field intensity (XOY-plane,  $z = 0$   
41 nm) by FDTD simulation with illumination source of 808 (Figure 2d), 980 (Figure 2e) and 1500  
42 nm (Figure 2f) are demonstrated by locating the  $\text{Cu}_7\text{S}_4@\text{Pd}$  nanocrystal in the center of a  
43 simulated box (Figure 2c). Control trials on Pd and  $\text{Cu}_7\text{S}_4$  were also performed (Figure S4-S5).  
44 Very weak LSPR feature was observed around the Pd nanoparticle at 808 nm, 980 nm, and 1500  
45 nm irradiation (Figure S4). Pd nanoparticles themselves barely have LSPR absorption at these  
46 three wavelengths, thus are unlikely the source of LSPR enhancement. Meanwhile,  $\text{Cu}_7\text{S}_4$   
47  
48  
49  
50  
51  
52  
53  
54  
55  
56  
57  
58  
59  
60

1  
2  
3 exhibits significant electrical field enhancement (Figure S5), with 1500 nm source triumphs  
4 other two wavelengths. Consequently the LSPR feature of the  $\text{Cu}_7\text{S}_4@Pd$  heteronanostructures is  
5  
6 mainly attributed to the  $\text{Cu}_7\text{S}_4$  domain. As for the  $\text{Cu}_7\text{S}_4@Pd$  heteronanostructures, there is an  
7  
8 apparent electrical field enhancement by all three wavelengths. In addition, the electrical field  
9  
10 intensity for 1500 nm irradiation appears far stronger than 808 and 980 nm, indicating the overall  
11  
12 LSPR of the heteronanostructure is more obvious if irradiation wavelength is close to the  $\text{Cu}_7\text{S}_4$   
13  
14 LSPR peak. In addition, enhanced LSPR feature around the Pd domain was observed, which may  
15  
16 be attributed to the extended influence from semiconductor domain to noble metal domain across  
17  
18 the interface. This result, together with our previous observation (Figure 2a), suggests a  
19  
20 promising pathway to effectively expand the localized electrical field enhancement from  $\text{Cu}_7\text{S}_4$   
21  
22 to the whole  $\text{Cu}_7\text{S}_4@Pd$  heteronanostructure, and offers potential to couple  $\text{Cu}_7\text{S}_4$  with other  
23  
24 metal catalysts without strong LSPR features.  
25  
26  
27  
28  
29  
30  
31  
32  
33  
34  
35  
36  
37  
38  
39  
40  
41  
42  
43  
44  
45  
46  
47  
48  
49  
50  
51  
52  
53  
54  
55  
56  
57  
58  
59  
60

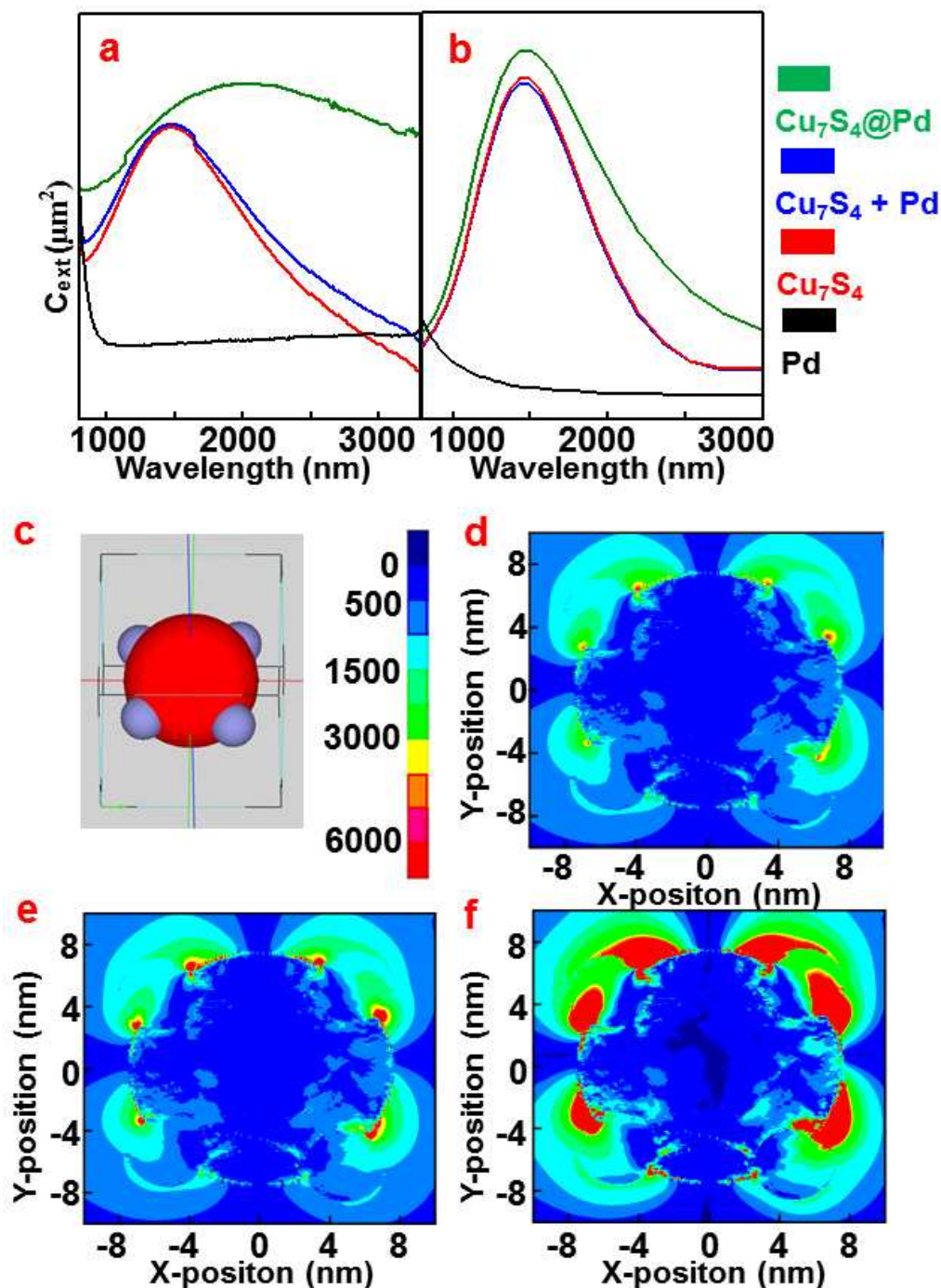


**Figure 2.** LSPR absorption spectra of different nanostructures obtained from experiment (a) and FDTD simulation (b). Green curves: Cu<sub>7</sub>S<sub>4</sub>@Pd heteronanostructures. Blue curves: physical mixture of Cu<sub>7</sub>S<sub>4</sub> and Pd nanoparticles. Red curves: Cu<sub>7</sub>S<sub>4</sub> nanoparticles. Black curves: Pd nanoparticles. (c) FDTD simulation setup for Cu<sub>7</sub>S<sub>4</sub>@Pd, and electrical field intensity scale. (d-f)

1  
2  
3 2D contour of the electric field intensities around the  $\text{Cu}_7\text{S}_4@\text{Pd}$  heteronanostructures under  
4 illumination of 808 nm (d), 980 nm (e) and 1500 nm (f), respectively.  
5  
6  
7  
8  
9

10  
11  
12 To assess catalytic activity of  $\text{Cu}_7\text{S}_4@\text{Pd}$ , Suzuki coupling reaction between iodobenzene and  
13 phenylboronic acid was used as the model reaction. The hydrophobic  $\text{Cu}_7\text{S}_4@\text{Pd}$  nanoparticles  
14 were dispersed into water with the help of cetyltrimethylammonium bromide (CTAB) (TEM  
15 image is shown in Figure S6). Given that 1500-nm diode laser is close to  $\text{Cu}_7\text{S}_4@\text{Pd}$  LSPR peak  
16 position, here we applied 1500-nm laser as illumination source in our trials. The concentration of  
17 the catalyst stock solution was quantified by inductively coupled plasma mass spectrometry  
18 (ICP-MS), and the dosage was carefully calculated prior to each test (Table S2). Initially, control  
19 experiments were carried out without laser irradiation nor heating. No traceable product was  
20 detected. Moreover, since our photocatalytic system is based on LSPR enhancement effect,  
21 photon utilization efficiency is determined dominantly by resonance frequency of  $\text{Cu}_7\text{S}_4@\text{Pd}$   
22 heteronanostructure. Irradiation source frequency at or close to intrinsic plasmon frequency on  
23  $\text{Cu}_7\text{S}_4@\text{Pd}$  heteronanostructure would benefit catalytic activity most. To verify this effect, we  
24 applied 808-nm, 980-nm and 1500-nm irradiation light for the Suzuki coupling reaction. The  
25 photocatalytic activities obtained in 1500-nm trial were much higher than those of 808-nm or  
26 980-nm trials at all three reaction time intervals (10 min, 20 min and 30 min). For example, with  
27 reaction time of 30 min, 1500-nm irradiation gave a 97% conversion (Figure 3a and Figure 3c-  
28 1), while 808-nm resulted in 45% conversion and 980-nm yielded slightly higher than 50%  
29 conversion (Figure 3a). When phenylboronic acid was replaced with *p*-tolylboronic acid, we also  
30 observed similar trend (Figure 3b).  
31  
32  
33  
34  
35  
36  
37  
38  
39  
40  
41  
42  
43  
44  
45  
46  
47  
48  
49  
50  
51  
52  
53  
54  
55  
56  
57  
58  
59  
60

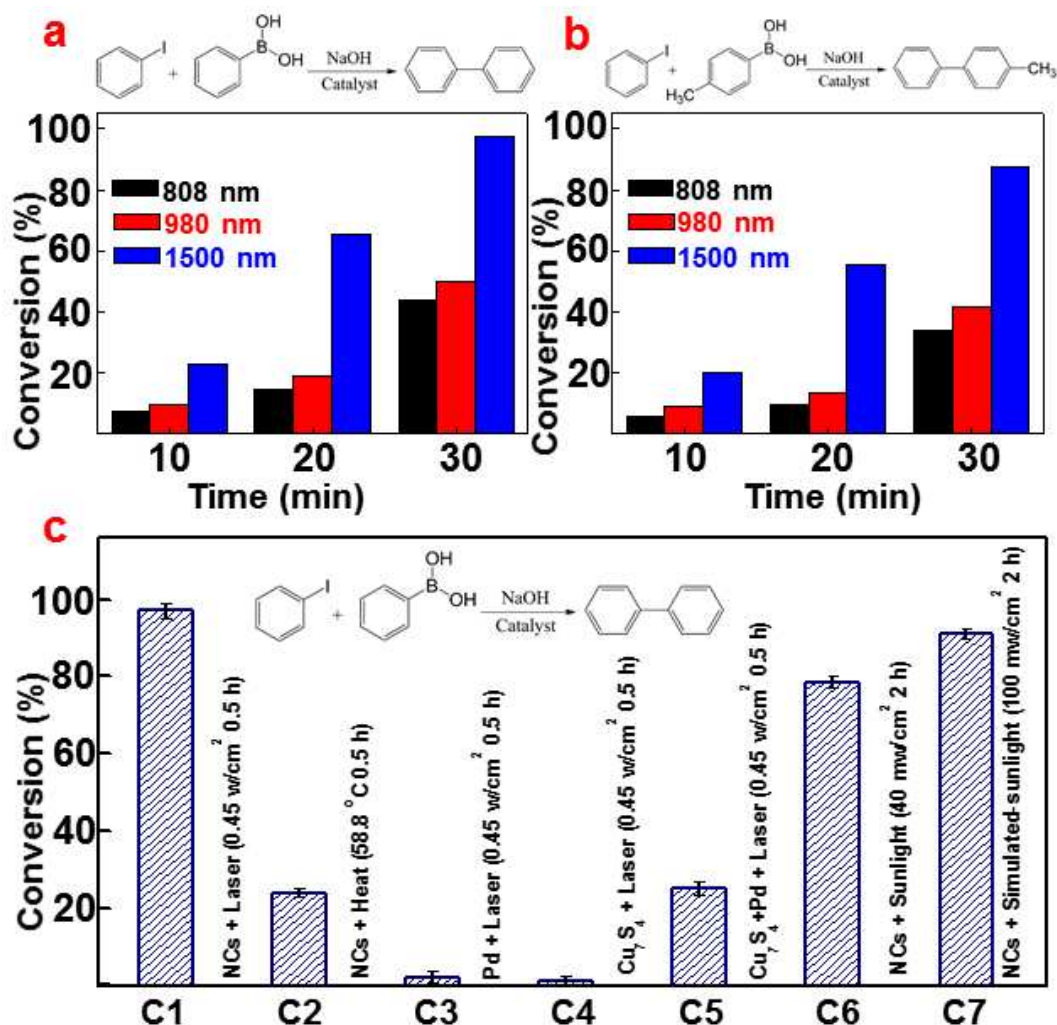


**Figure 3.** The photocatalytic activity of Cu<sub>7</sub>S<sub>4</sub>@Pd nanostructure for Suzuki coupling reactions of iodobenzene with different reagents: (a) phenylboronic acid and (b) *p*-tolylboronic acid. Both reactions were under 808-nm, 980-nm and 1500-nm laser irradiation for 30 min. The power density of each laser source is 0.45 W/cm<sup>2</sup>. (c) Conversion comparison with different catalysts under various catalytic conditions. All lasers used here is the 1500-nm laser.

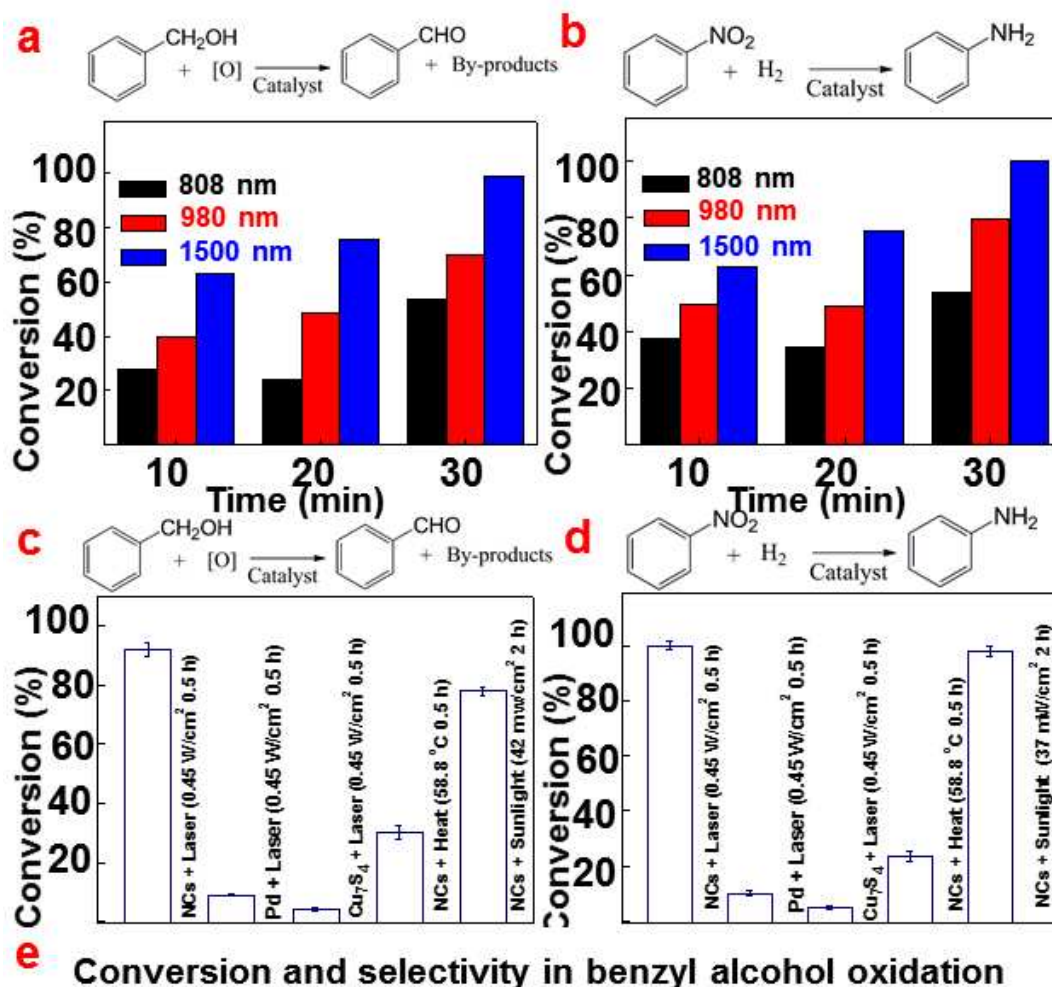
It is generally recognized that extensive LSPR features can give rise to photocatalysis and photothermal effect simultaneously.<sup>10, 54</sup> In order to evaluate influence of these two effects, we

1  
2  
3 used conventional heating as comparison tests. We began to record temperature changes with  
4  
5 1500-nm laser irradiation ( $0.45 \text{ W/cm}^2$ ), and found the temperature raised and kept at  $58.8 \text{ }^\circ\text{C}$   
6  
7 within 5 min (Figure S7). Thus we ran the reaction with  $\text{Cu}_7\text{S}_4@\text{Pd}$  heteronanostructures at  $58.8$   
8  
9  $^\circ\text{C}$  for 30 min in dark environment (Figure 3c-2). Less than 25% conversion was recorded. This  
10  
11 is substantially different from nearly 100% conversion provided by laser irradiation, from which  
12  
13 we can conclude that photothermal effect only contributes to part of the catalytic effect, while  
14  
15 photocatalysis serves as prevailing factor to determine overall activity.  
16  
17  
18  
19  
20  
21  
22  
23

24 Additionally, to prove the synergetic effect of  $\text{Cu}_7\text{S}_4$  and Pd nanostructures as an integrated  
25  
26 system, we conducted reactions based on Pd nanoparticles alone,  $\text{Cu}_7\text{S}_4$  nanoparticles alone and  
27  
28 physical mixture of the two (no chemical bonding between two components like in  $\text{Cu}_7\text{S}_4@\text{Pd}$ ).  
29  
30 It can be seen in Figures 3c-3 and 3c-4, neither Pd-only trial nor  $\text{Cu}_7\text{S}_4$ -only trial exhibited yield  
31  
32 higher than 10%. These results can be interpreted as follows: the Pd domain has little  
33  
34 contribution to the NIR LSPR effects, and  $\text{Cu}_7\text{S}_4$  alone has limited catalytic effect in the Suzuki  
35  
36 coupling reaction. The mixture of these two components achieved  $\sim 32\%$  conversion (Figure 3c-  
37  
38 5), which is far lower than that from  $\text{Cu}_7\text{S}_4@\text{Pd}$  (nearly 100% converted). This is a strong proof  
39  
40 that intimate vicinity between  $\text{Cu}_7\text{S}_4$  and Pd domains is crucial, and the photocatalysis is a  
41  
42 synergetic outcome of integrated  $\text{Cu}_7\text{S}_4$  and Pd components.  
43  
44  
45  
46  
47  
48  
49  
50  
51

52 To evaluate the effectiveness of the  $\text{Cu}_7\text{S}_4@\text{Pd}$  heteronanostructures in other reactions, we  
53  
54 further assessed them in the selective oxidation of benzyl alcohol and the hydrogenation of  
55  
56 nitrobenzene. Firstly we examined the plasmon enhancement effect on these two reactions  
57  
58  
59  
60

1  
2  
3 through wavelength dependent studies. 808-nm, 980-nm and 1500-nm sources were used. In  
4  
5 both oxidation and hydrogenation reaction trials, 1500-nm trials demonstrated best conversions,  
6  
7 followed by 980-nm, and then the 808-nm (Figure 4a-b). Similar to wavelength-dependent  
8  
9 results obtained in the Suzuki coupling reaction, these results clearly show the plasmon  
10  
11 resonance enhancement near the LSPR peak exhibits predominant influence in photocatalytic  
12  
13 process. Again, the photothermal effect still serves as minor effect compared to that of  
14  
15 photocatalysis. In oxidation reaction, direct heating the reaction solution at 58.8 °C gave  
16  
17 conversion of less than 30%, and in reduction reaction the conversion under identical  
18  
19 conventional heating condition was 22% (Figure 4c-d). Neither of them is comparable to near  
20  
21 100% conversion obtained under 1500-nm irradiation (Figure 4c-d). In addition, we used pure Pd  
22  
23 and Cu<sub>7</sub>S<sub>4</sub> to conduct control experiments. In both oxidation and reduction reactions, Pd or Cu<sub>7</sub>S<sub>4</sub>  
24  
25 nanocatalysts yielded less than 10% conversion with 1500-nm irradiation (Figure 4c-d).  
26  
27 Moreover, we found that in the benzyl alcohol oxidation reaction products, *i.e.* benzaldehyde,  
28  
29 benzyl benzoate and benzoic acid (Figure 4e), 1500-nm source yielded 99.57% selectivity  
30  
31 towards benzaldehyde, while 808-nm and 980-nm gave 95.87% and 93.43% selectivity,  
32  
33 respectively. The selectivity towards benzyl benzoate also changes significantly with respect to  
34  
35 wavelengths. The selectivity of 3.90% was obtained for 808-nm trial, 5.62% for 980-nm trial and  
36  
37 merely 0.28% for 1500-nm trial.  
38  
39  
40  
41  
42  
43  
44  
45  
46  
47  
48  
49  
50  
51  
52  
53  
54  
55  
56  
57  
58  
59  
60



Wavelength (nm)	Conversion (%)	Selectivity (%)		
		<i>Benzaldehyde</i>	<i>Benzyl benzoate</i>	<i>Benzoic acid</i>
808	53.63	95.87	3.90	0.23
980	69.75	93.43	5.62	0.95
1500	99.72	99.57	0.28	0.15

**Figure 4.** The photocatalytic activities of  $\text{Cu}_7\text{S}_4@\text{Pd}$  in (a) selective oxidation of benzyl alcohol and (b) hydrogenation of nitrobenzene, under 808-nm, 980-nm and 1500-nm irradiation. The power density for three wavelength lasers is  $0.45 \text{ W/cm}^2$ . (c) Conversion comparison of different catalysts under different catalytic conditions in selective oxidation of benzyl alcohol. (d)

1  
2  
3 Conversion comparison of different catalysts under different catalytic conditions in reduction of  
4 nitrobenzene. (e) Products selectivity profile in selective oxidation of benzyl alcohol using  
5  
6 different irradiation wavelengths.  
7  
8  
9

10  
11  
12 We further carried out the catalytic reaction with simulated sunlight source to examine the  
13 pragmatic feasibility of our photocatalyst. After being exposed to the simulated sunlight (100  
14 mW/cm<sup>2</sup>) for 2 hours, nearly 96% conversion was observed for Suzuki coupling reaction (Figure  
15 3c-7). Inspired by this promising result, we also conducted the solar photocatalysis reaction with  
16 real sunlight. Under the typical solar irradiation in local outdoor environment (the average solar  
17 power density was 40 mW/cm<sup>2</sup>), 78.6% iodobenzene was converted to biphenyl after 2 hours'  
18 exposure (Figure 3c-6). In benzyl alcohol oxidation reaction, 77.8% conversion was obtained  
19 (the average solar power density was 42 mW/cm<sup>2</sup>), and ~97% conversion in nitrobenzene  
20 hydrogenation was achieved with average solar power density of 37 mW/cm<sup>2</sup> (Figure 4c-d). In  
21 addition, the recyclability tests based on Suzuki coupling reaction revealed that the  
22 photocatalytic efficiency and catalyst morphology preserved after five cycles, which is desirable  
23 with respect to economical consideration (Figure S8). Lastly, since our synthetic protocol can be  
24 extended to Cu<sub>7</sub>S<sub>4</sub>@Pt, Cu<sub>7</sub>S<sub>4</sub>@Au and Cu<sub>7</sub>S<sub>4</sub>@Ag, we assessed their catalytic performances  
25 through oxidation and reduction reactions under sunlight for 2 hours (the average solar power  
26 density was 47.5 mW/cm<sup>2</sup>). Our results indicated they all display fairly good catalytic activities  
27 (Figure S9).  
28  
29  
30  
31  
32  
33  
34  
35  
36  
37  
38  
39  
40  
41  
42  
43  
44  
45  
46  
47  
48  
49  
50  
51  
52  
53  
54  
55  
56  
57  
58  
59  
60

1  
2  
3  
4 In order to explain the photocatalytic enhancement mechanism, we measured band structure of  
5  
6  $\text{Cu}_7\text{S}_4$ . The indirect and direct band gap of  $\text{Cu}_7\text{S}_4$  was determined by Kubelka-Munk method<sup>62</sup> as  
7  
8 0.821 eV and 1.432 eV, respectively (Figure 5a-b). Valence band position was detected via  
9  
10 electrochemical method<sup>62</sup> and calculated as -5.316 eV (Figure 5c-d). Furthermore, the gap  
11  
12 between the top of valence band and Fermi level of  $\text{Cu}_7\text{S}_4$  is estimated to be 0.125 eV (see  
13  
14 Supporting Information for calculation), *i.e.* the Fermi level of  $\text{Cu}_7\text{S}_4$  ( $E_F = -5.191$  eV) is above  
15  
16 and close to its valence band, representing a typical p-type semiconductor (Figure 5e).<sup>58</sup> As the  
17  
18 experimental results suggest that reactions illuminated by 1500 nm (~0.826 eV, close to LSRP  
19  
20 peak) show far higher conversion rate than those by 808 nm (1.534 eV) and 980 nm (1.265 eV),  
21  
22 it is unlikely that the interband transition has major effect on the catalytic reactions. We suggest  
23  
24 that under 1500 nm illumination, LSRP absorption of  $\text{Cu}_7\text{S}_4$  generates “hot holes”, which  
25  
26 possess sufficient energy to overcome the small Schottky barrier and inject into Pd domain. It is  
27  
28 possible the hot-hole injection renders the Pd surface electron-deficient, which then serves as a  
29  
30 key contribution to the observed photocatalytic enhancement effect for  $\text{Cu}_7\text{S}_4@Pd$ . This  
31  
32 hypothesis matches reasonably well with our experimental results. In terms of Suzuki coupling  
33  
34 reaction, theoretical studies indicated that the rate-limiting step is the oxidative addition of aryl  
35  
36 halides onto Pd(0).<sup>63</sup> This process favors the positively charged Pd surface, which resembles  
37  
38 electron-withdrawing ligands and can promote activation of aryl halides.<sup>63</sup> In the catalytic  
39  
40 oxidation of benzyl alcohol, hot holes injected to Pd domain might function like oxidant and  
41  
42 react *in-situ* with benzyl alcohol and the derivative species adsorbed on Pd surface, so as to  
43  
44 accelerate the reaction. In the hydrogenation reaction, Pd is generally considered active catalyst  
45  
46 but suffers from rapid surface-poisoning due to strong binding of H atoms.<sup>64,65</sup> Previous studies  
47  
48 suggested negative charges enhanced the binding of H atoms on Pd surface, while positive  
49  
50  
51  
52  
53  
54  
55  
56  
57  
58  
59  
60

1  
2  
3 charges help with dissociation of adsorbed H atoms.<sup>64</sup> Hence, we propose the transferred hot  
4  
5 holes can facilitate hydrogenation reaction through promoting H atom dissociation and thus keep  
6  
7  
8 Pd surface consistently active, leading to enhanced catalyst activity.  
9  
10  
11  
12  
13  
14  
15  
16  
17  
18  
19  
20  
21  
22  
23  
24  
25  
26  
27  
28  
29  
30  
31  
32  
33  
34  
35  
36  
37  
38  
39  
40  
41  
42  
43  
44  
45  
46  
47  
48  
49  
50  
51  
52  
53  
54  
55  
56  
57  
58  
59  
60

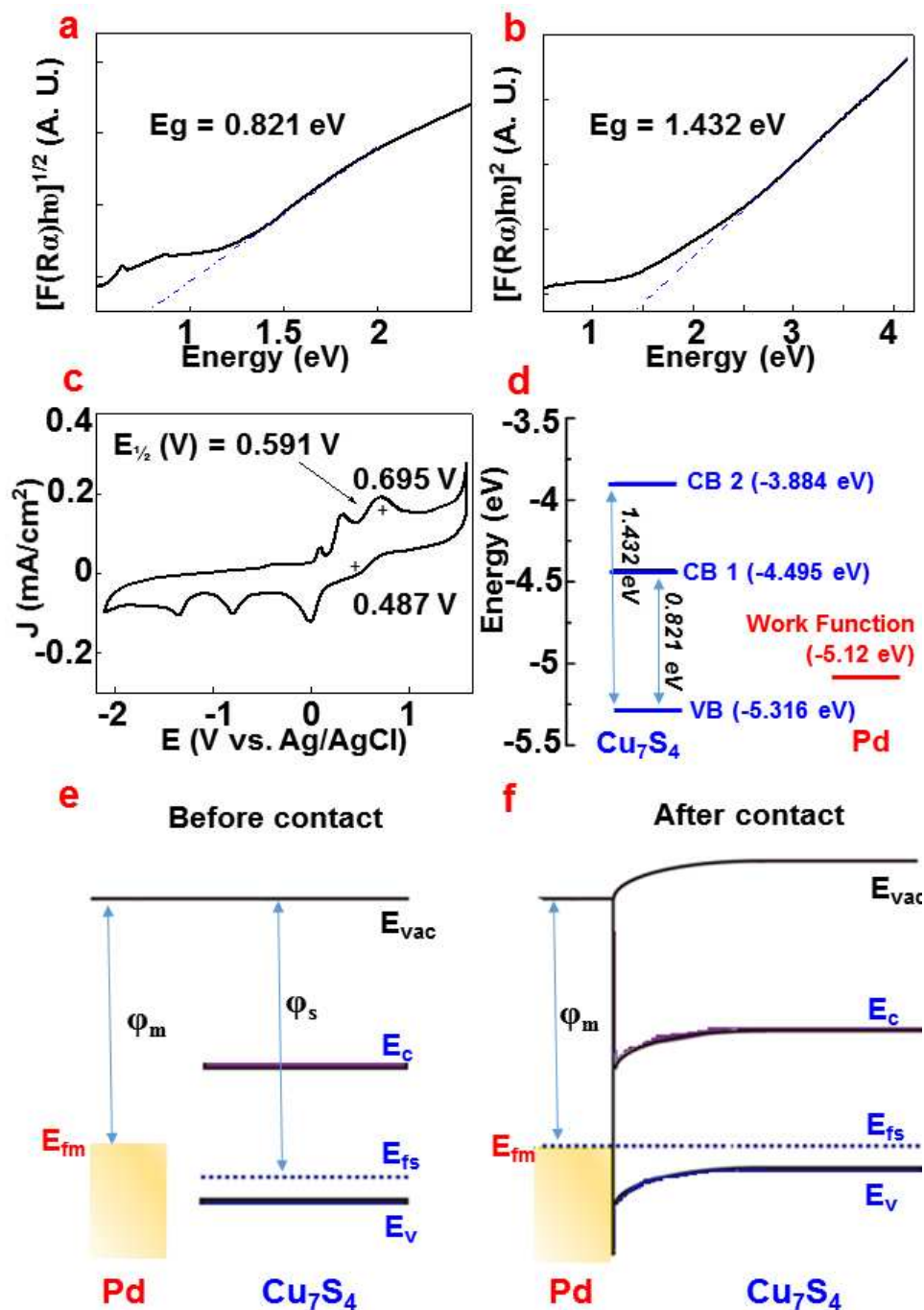


**Figure 5.** Plots of the indirect (a) and direct (b) band gap of  $\text{Cu}_7\text{S}_4$ . (c) The cyclic voltammograms of  $\text{Cu}_7\text{S}_4$ . (d) The energy level line-up of  $\text{Cu}_7\text{S}_4$ . (e-f) Energy band diagram of metal (Pd) and p-type semiconductor ( $\text{Cu}_7\text{S}_4$ ) before (e) and after (f) contact.  $E_g$ : band gap.  $E_{vac}$ : vacuum energy.  $E_c$ : conduction band position.  $E_v$ : valence band position.  $\phi_m$ : metal work

1  
2  
3 function.  $\phi_s$ : semiconductor work function.  $E_{fm}$ : metal Fermi level.  $E_{fs}$ : semiconductor Fermi  
4  
5 level.  
6  
7

8  
9  
10 In conclusion, we have developed a facile strategy for the synthesis of  $\text{Cu}_7\text{S}_4@\text{Pd}$   
11 heteronanostructures with excellent NIR LSPR properties and photocatalytic activities. This  
12 synthetic method can be easily extended to other semiconductor-metal heteronanostructures. The  
13  $\text{Cu}_7\text{S}_4$  semiconductor domain acts as a plasmonic component for efficient photo-harvesting in  
14  
15 NIR region, while the Pd noble metal domain provides active sites for organic reactions.  
16  
17 Experiment results indicate  $\text{Cu}_7\text{S}_4$  and Pd domains function as a synergetic system. Upon 1500-  
18  
19 nm irradiation and LSPR absorption, hot-holes can be generated on  $\text{Cu}_7\text{S}_4$ , which can inject into Pd  
20  
21 domain to render hole-rich Pd surface. This hole-rich Pd surface may serve as effective catalytic  
22  
23 sites for Suzuki coupling, oxidation and reduction reactions. Furthermore, unlike most of the  
24  
25 traditional semiconductor-metal hybrid photocatalysts in which the LSPR of the noble metal  
26  
27 nanoparticles assist the visible range absorption of the semiconductor, here  $\text{Cu}_7\text{S}_4$  nanoparticle  
28  
29 utilizes NIR range photon through LSPR and extends the benefits to the metal catalyst. This  
30  
31 leads to exciting potentials in photocatalysis especially considering that  $\text{Cu}_7\text{S}_4$  has been reported  
32  
33 to demonstrate tunable LSPR at different carrier densities.<sup>52</sup> Although the exact mechanism and  
34  
35 the synergetic roles of  $\text{Cu}_7\text{S}_4$  and Pd in these photocatalytic reactions need further investigations,  
36  
37 this study opens up wide possibilities in utilizing NIR LSPR properties of Copper Chalcogenides  
38  
39 to enhance photocatalysis. Furthermore, incorporation of various metal nanocatalysts with  $\text{Cu}_7\text{S}_4$   
40  
41 is expected to broaden materials choice and hence exhibit more fascinating catalytic  
42  
43 performances.  
44  
45  
46  
47  
48  
49  
50  
51  
52  
53  
54  
55  
56  
57  
58  
59  
60

## ASSOCIATED CONTENT

**Supporting Information.** Detailed experimental procedures, equipment list, simulation setup and theoretical calculation steps; TEM images of  $\text{Cu}_7\text{S}_4$  and Pd nanoparticles (Figure S1); Standard XRD peak locations of  $\text{Cu}_x\text{S}$  (Table S1); TEM, HRTEM images and respective XRD patterns of  $\text{Cu}_7\text{S}_4@\text{Au}$ ,  $\text{Cu}_7\text{S}_4@\text{Pt}$ , and  $\text{Cu}_7\text{S}_4@\text{Ag}$  heteronanostructures (Figure S2-3); FDTD simulation results for Pd and  $\text{Cu}_7\text{S}_4$  nanoparticle with different irradiation wavelengths (Figure S4-S5); TEM images of  $\text{Cu}_7\text{S}_4@\text{Pd}$  heteronanostructures in aqueous solution (Figure S6); The catalyst dosage applied in reactions (Table S2); Reaction solution temperature change with respect to time under irradiation of different wavelengths (Figure S7); The recyclability test result and TEM image of  $\text{Cu}_7\text{S}_4@\text{Pd}$  after reactions (Table S8); The photocatalytic performance of  $\text{Cu}_7\text{S}_4@\text{Pt}$ ,  $\text{Cu}_7\text{S}_4@\text{Au}$ , and  $\text{Cu}_7\text{S}_4@\text{Ag}$  (Figure S9). This material is available free of charge via the Internet at <http://pubs.acs.org>.

## AUTHOR INFORMATION

### Corresponding Author

E-mail: lywang@mail.buct.edu.cn; yhuang@seas.ucla.edu.

### Author Contributions

All authors contributed to the preparation of this manuscript. L. W. conceived the idea. J. C., L. C., J. X., J. M., G. F. and L. W. performed experiments, data collection, analysis, and explanation. L.L. and L. Z. helped with simulation. Y. L., E. Z., H. W. and Y. H. helped with design of the experiments, data analysis, and organization of manuscript. All authors have given approval to the final version.

## Notes

The authors declare no competing financial interest.

## ACKNOWLEDGMENT

The authors gratefully acknowledge the financial support by the National Natural Science Foundation of China (21475007 and 21275015), the State Key Project of Fundamental Research of China (2011CB932403). L.W. acknowledges the support from the “Innovation and Promotion Project of Beijing University of Chemical Technology” and the “Public Hatching Platform for Recruited Talents of Beijing University of Chemical Technology”. Y.H. acknowledges support from ARO through Award No. 54709-MS-PCS.

## REFERENCES

1. Navalon, S.; de Miguel, M.; Martin, R.; Alvaro, M.; Garcia, H. *J. Am. Chem. Soc.* **2011**, *133*, 2218-2226.
2. Eley, C.; Li, T.; Liao, F. L.; Fairclough, S. M.; Smith, J. M.; Smith, G.; Tsang, S. C. E. *Angew. Chem.-Int. Edit.* **2014**, *53*, 7838-7842.
3. Li, P.; Wei, Z.; Wu, T.; Peng, Q.; Li, Y. D. *J. Am. Chem. Soc.* **2011**, *133*, 5660-5663.
4. Attia, Y. A.; Buceta, D.; Blanco-Varela, C.; Mohamed, M. B.; Barone, G.; Lopez-Quintela, M. A. *J. Am. Chem. Soc.* **2014**, *136*, 1182-1185.
5. Zheng, Z. K.; Tachikawa, T.; Majima, T. *J. Am. Chem. Soc.* **2014**, *136*, 6870-6873.
6. Yu, X. L.; Shavel, A.; An, X. Q.; Luo, Z. S.; Ibanez, M.; Cabot, A. *J. Am. Chem. Soc.* **2014**, *136*, 9236-9239.
7. Zhang, S.; Metin, O.; Su, D.; Sun, S. H. *Angew. Chem.-Int. Edit.* **2013**, *52*, 3681-3684.
8. Choi, C.; Feng, J.; Li, Y. G.; Wu, J.; Zak, A.; Tenne, R.; Dai, H. *J. Nano Res.* **2013**, *6*, 921-928.
9. Yahaya, A. H.; Gondal, M. A.; Hameed, A. *Chem. Phys. Lett.* **2004**, *400*, 206-212.
10. Huang, X. Q.; Li, Y. J.; Chen, Y.; Zhou, H. L.; Duan, X. F.; Huang, Y. *Angew. Chem.-Int. Edit.* **2013**, *52*, 6063-6067.
11. Huang, X. Q.; Li, Y. J.; Chen, Y.; Zhou, E. B.; Xu, Y. X.; Zhou, H. L.; Duan, X. F.; Huang, Y. *Angew. Chem.-Int. Edit.* **2013**, *52*, 2520-2524.
12. Huang, X. Q.; Zhu, E. B.; Chen, Y.; Li, Y. J.; Chiu, C. Y.; Xu, Y. X.; Lin, Z. Y.; Duan, X. F.; Huang, Y. *Adv. Mater.* **2013**, *25*, 2974-2979.

13. Huang, X. Q.; Tang, S. H.; Mu, X. L.; Dai, Y.; Chen, G. X.; Zhou, Z. Y.; Ruan, F. X.; Yang, Z. L.; Zheng, N. F. *Nature Nanotechnology* **2011**, *6*, 28-32.
14. Zhang, H.; Jin, M. S.; Wang, J. G.; Li, W. Y.; Camargo, P. H. C.; Kim, M. J.; Yang, D. R.; Xie, Z. X.; Xia, Y. A. *J. Am. Chem. Soc.* **2011**, *133*, 6078-6089.
15. Xia, X. H.; Figueroa-Cosme, L.; Tao, J.; Peng, H. C.; Niu, G. D.; Zhu, Y. M.; Xia, Y. N. *J. Am. Chem. Soc.* **2014**, *136*, 10878-10881.
16. Chiu, C. Y.; Li, Y. J.; Ruan, L. Y.; Ye, X. C.; Murray, C. B.; Huang, Y. *Nat. Chem.* **2011**, *3*, 393-399.
17. Jia, Y. Y.; Jiang, Y. Q.; Zhang, J. W.; Zhang, L.; Chen, Q. L.; Xie, Z. X.; Zheng, L. S. *J. Am. Chem. Soc.* **2014**, *136*, 3748-3751.
18. Wu, Y. E.; Wang, D. S.; Niu, Z. Q.; Chen, P. C.; Zhou, G.; Li, Y. D. *Angew. Chem.-Int. Edit.* **2012**, *51*, 12524-12528.
19. Li, L. L.; Chen, X. B.; Wu, Y. E.; Wang, D. S.; Peng, Q.; Zhou, G.; Li, Y. D. *Angew. Chem.-Int. Edit.* **2013**, *52*, 11049-11053.
20. Xie, S. F.; Zhang, H.; Lu, N.; Jin, M. S.; Wang, J. G.; Kim, M. J.; Xie, Z. X.; Xia, Y. N. *Nano Lett.* **2013**, *13*, 6262-6268.
21. Hong, X.; Wang, D. S.; Cai, S. F.; Rong, H. P.; Li, Y. D. *J. Am. Chem. Soc.* **2012**, *134*, 18165-18168.
22. Chen, C.; Kang, Y. J.; Huo, Z. Y.; Zhu, Z. W.; Huang, W. Y.; Xin, H. L. L.; Snyder, J. D.; Li, D. G.; Herron, J. A.; Mavrikakis, M.; Chi, M. F.; More, K. L.; Li, Y. D.; Markovic, N. M.; Somorjai, G. A.; Yang, P. D.; Stamenkovic, V. R. *Science* **2014**, *343*, 1339-1343.
23. Xie, S. F.; Lu, N.; Xie, Z. X.; Wang, J. G.; Kim, M. J.; Xia, Y. N. *Angew. Chem.-Int. Edit.* **2012**, *51*, 10266-10270.
24. Blankenship, R. E.; Tiede, D. M.; Barber, J.; Brudvig, G. W.; Fleming, G.; Ghirardi, M.; Gunner, M. R.; Junge, W.; Kramer, D. M.; Melis, A.; Moore, T. A.; Moser, C. C.; Nocera, D. G.; Nozik, A. J.; Ort, D. R.; Parson, W. W.; Prince, R. C.; Sayre, R. T. *Science* **2011**, *332*, 805-809.
25. Linic, S.; Christopher, P.; Ingram, D. B. *Nat. Mater.* **2011**, *10*, 911-921.
26. Christopher, P.; Xin, H. L.; Linic, S. *Nat. Chem.* **2011**, *3*, 467-472.
27. Wang, F.; Li, C. H.; Chen, H. J.; Jiang, R. B.; Sun, L. D.; Li, Q.; Wang, J. F.; Yu, J. C.; Yan, C. H. *J. Am. Chem. Soc.* **2013**, *135*, 5588-5601.
28. Gao, H. W.; Liu, C.; Jeong, H. E.; Yang, P. D. *ACS Nano* **2012**, *6*, 234-240.
29. Zhang, T. T.; Zhao, H. Y.; He, S. N.; Liu, K.; Liu, H. Y.; Yin, Y. D.; Gao, C. B. *ACS Nano* **2014**, *8*, 7297-7304.
30. Zedan, A. F.; Moussa, S.; Ternner, J.; Atkinson, G.; El-Shall, M. S. *ACS Nano* **2013**, *7*, 627-636.
31. Xia, Y. N.; Li, W. Y.; Cogley, C. M.; Chen, J. Y.; Xia, X. H.; Zhang, Q.; Yang, M. X.; Cho, E. C.; Brown, P. K. *Accounts Chem. Res.* **2011**, *44*, 914-924.
32. Dasgupta, N. P.; Liu, C.; Andrews, S.; Prinz, F. B.; Yang, P. D. *J. Am. Chem. Soc.* **2013**, *135*, 12932-12935.
33. Zhang, H.; Li, Y. J.; Ivanov, I. A.; Qu, Y. Q.; Huang, Y.; Duan, X. F. *Angew. Chem.-Int. Edit.* **2010**, *49*, 2865-2868.
34. Tu, N. N.; Wang, L. Y. *Chem. Commun.* **2013**, *49*, 6319-6321.
35. Bardhan, R.; Lal, S.; Joshi, A.; Halas, N. J. *Accounts Chem. Res.* **2011**, *44*, 936-946.
36. Jain, P. K.; Huang, X. H.; El-Sayed, I. H.; El-Sayed, M. A. *Accounts Chem. Res.* **2008**, *41*, 1578-1586.

37. Primo, A.; Marino, T.; Corma, A.; Molinari, R.; Garcia, H. *J. Am. Chem. Soc.* **2011**, *133*, 6930-6933.
38. Zahran, E. M.; Bedford, N. M.; Nguyen, M. A.; Chang, Y. J.; Guiton, B. S.; Naik, R. R.; Bachas, L. G.; Knecht, M. R. *J. Am. Chem. Soc.* **2014**, *136*, 32-35.
39. Long, R.; Prezhdo, O. V. *J. Am. Chem. Soc.* **2014**, *136*, 4343-4354.
40. Yamada, Y.; Tsung, C. K.; Huang, W.; Huo, Z. Y.; Habas, S. E.; Soejima, T.; Aliaga, C. E.; Somorjai, G. A.; Yang, P. D. *Nat. Chem.* **2011**, *3*, 372-376.
41. Wu, K. F.; Zhu, H. M.; Liu, Z.; Rodriguez-Cordoba, W.; Lian, T. Q. *J. Am. Chem. Soc.* **2012**, *134*, 10337-10340.
42. He, W. W.; Kim, H. K.; Warner, W. G.; Melka, D.; Callahan, J. H.; Yin, J. J. *J. Am. Chem. Soc.* **2014**, *136*, 750-757.
43. Kuo, C. H.; Yang, Y. C.; Gwo, S.; Huang, M. H. *J. Am. Chem. Soc.* **2011**, *133*, 1052-1057.
44. Cho, S.; Lee, M. J.; Kim, M. S.; Lee, S.; Kim, Y. K.; Lee, D. H.; Lee, C. W.; Cho, K. H.; Chung, J. H. *J. Dermatol. Sci.* **2008**, *50*, 123-133.
45. Tian, Q. W.; Hu, J. Q.; Zhu, Y. H.; Zou, R. J.; Chen, Z. G.; Yang, S. P.; Li, R. W.; Su, Q. Q.; Han, Y.; Liu, X. G. *J. Am. Chem. Soc.* **2013**, *135*, 8571-8577.
46. Hsu, S. W.; On, K.; Tao, A. R. *J. Am. Chem. Soc.* **2011**, *133*, 19072-19075.
47. Han, W.; Yi, L. X.; Zhao, N.; Tang, A. W.; Gao, M. Y.; Tang, Z. Y. *J. Am. Chem. Soc.* **2008**, *130*, 13152-13161.
48. Han, S. K.; Gong, M.; Yao, H. B.; Wang, Z. M.; Yu, S. H. *Angew. Chem.-Int. Edit.* **2012**, *51*, 6365-6368.
49. Ding, X.; Liow, C. H.; Zhang, M.; Huang, R.; Li, C.; Shen, H.; Liu, M.; Zou, Y.; Gao, N.; Zhang, Z.; Li, Y.; Wang, Q.; Li, S.; Jiang, J. *J. Am. Chem. Soc.* **2014**, *136*, 15684-93.
50. Cui, J. B.; Jiang, R.; Xu, S. Y.; Hu, G. F.; Wang, L. Y. *Small* **2015**, *11*, 10.1002/smll.201500845.
51. Subramanian, V.; Wolf, E. E.; Kamat, P. V. *J. Am. Chem. Soc.* **2004**, *126*, 4943-4950.
52. Luther, J. M.; Jain, P. K.; Ewers, T.; Alivisatos, A. P. *Nat. Mater.* **2011**, *10*, 361-366.
53. Shaviv, E.; Schubert, O.; Alves-Santos, M.; Goldoni, G.; Di Felice, R.; Vallee, F.; Del Fatti, N.; Banin, U.; Sonnichsen, C. *ACS Nano* **2011**, *5*, 4712-4719.
54. Banin, U.; Ben-Shahar, Y.; Vinokurov, K. *Chem. Mat.* **2014**, *26*, 97-110.
55. Toshima, N.; Yonezawa, T. *New J. Chem.* **1998**, 1179-1201.
56. Kim, S. M.; Lee, S. J.; Kim, S. H.; Kwon, S.; Yee, K. J.; Song, H.; Somorjai, G. A.; Park, J. Y. *Nano Lett.* **2013**, *13*, 1352-1358.
57. Kriegel, I.; Rodriguez-Fernandez, J.; Da Como, E.; Lutich, A. A.; Szeifert, J. M.; Feldmann, J. *Chem. Mat.* **2011**, *23*, 1830-1834.
58. Wang, S.; Riedinger, A.; Li, H.; Fu, C.; Liu, H.; Li, L.; Liu, T.; Tan, L.; Barthel, M. J.; Pugliese, G.; De. Donato, F.; D'Abbusco, M. S.; Meng, X.; Manna, L.; Meng, H.; Pellegrino, T. *ACS Nano* **2015**, *9*, 1788-1800.
59. Mukherjee, S.; Libisch, F.; Large, N.; Neumann, O.; Brown, L. V.; Cheng, J.; Lassiter, J. B.; Carter, E. A.; Nordlander, P.; Halas, N. J. *Nano Lett.* **2013**, *13*, 240-247.
60. Li, J. T.; Cushing, S. K.; Bright, J.; Meng, F. K.; Senty, T. R.; Zheng, P.; Bristow, A. D.; Wu, N. Q. *ACS Catal.* **2013**, *3*, 47-51.
61. Simon, T.; Bouchonville, N.; Berr, M. J.; Vaneski, A.; Adrovic, A.; Volbers, D.; Wyrwich, R.; Doblinger, M.; Susha, A. S.; Rogach, A. L.; Jackel, F.; Stolarczyk, J. K.; Feldmann, J. *Nat. Mater.* **2014**, *13*, 1013-1018.

- 1  
2  
3  
4  
5  
6  
7  
8  
9  
10  
11  
12  
13  
14  
15  
16  
17  
18  
19  
20  
21  
22  
23  
24  
25  
26  
27  
28  
29  
30  
31  
32  
33  
34  
35  
36  
37  
38  
39  
40  
41  
42  
43  
44  
45  
46  
47  
48  
49  
50  
51  
52  
53  
54  
55  
56  
57  
58  
59  
60
62. Kim, Y.; Park, K. Y.; Jang, D. M.; Song, Y. M.; Kim, H. S.; Cho, Y. J.; Myung, Y.; Park, J. J. *Phys. Chem. C* **2010**, *114*, 22141-22146.
63. Norio, M.; Akira, S. *Chemical Reviews*. **1995**, *95*, 2457-2483
64. Long, R.; Rao, Z. L.; Mao, K. K.; Li, Y.; Zhang, C.; Liu, Q. L.; Wang, C. M.; Li, Z. Y.; Wu, X. J.; Xiong, Y. J. *Angew. Chem.-Int. Edit.* **2015**, *54*, 2425-2430
65. Bai, S.; Jiang, J.; Zhang, Q.; Xiong, Y. J. *Chemical Society reviews*. **2015**, *44*, 2839-2939.

## Table of Contents

Cu<sub>7</sub>S<sub>4</sub>@Pd heteronanostructures are synthesized and used as LSPR enhanced photocatalyst. It is proved effective in Suzuki coupling reaction, selective oxidation of benzyl alcohol, and hydrogenation of nitrobenzene. Extensive hot-hole generation on Cu<sub>7</sub>S<sub>4</sub> and subsequent injection into Pd domain under laser irradiation with wavelength close to the LSPR peak is believed the main reason of this high photocatalytic activity.

